

Last generation instrument for agriculture multispectral data collection

Marco Dubbini¹, Andrea Pezzuolo², Michaela De Giglio³, Mario Gattelli⁴,
Lucia Curzio⁴, Daniele Covi⁵, Tatevik Yezekyan⁶, Francesco Marinello^{2,7*}

(1. Department of History and Cultures, University of Bologna, 40126 Bologna, Italy;

2. Department of Land, Environment, Agriculture and Forestry, University of Padova, 35020 Legnaro, Padova, Italy;

3. Department of Civil, Chemical, Environmental and Materials Engineering, University of Bologna, 40126 Bologna, Italy;

4. SAL Engineering srl, 48026 Russi, Ravenna, Italy; 5. Eoptis srl, 38121 Trento, Italy;

6. Estonian University of Life Sciences, 51014 Tartu, Estonia; 7. NEOS srl, Spin off of the University of Padova, 35129 Padova, Italy)

Abstract: In recent years, the acquisition and analysis of multispectral data are gaining a growing interest and importance in agriculture. On the other hand, new technologies are opening up for the possibility of developing and implementing sensors with relatively small size and featuring high technical performances. Thanks to low weights and high signal to noise ratios, such sensors can be transported by different types of means (terrestrial as well as aerial vehicles), giving new opportunities for assessment and monitoring of several crops at different growing stages or health conditions. The choice and specialization of individual bands, within the electromagnetic spectrum ranging from the ultraviolet to the infrared, plays a fundamental role in the definition of the so-called vegetation indices (eg. NDVI, GNDVI, SAVI, and dozens of others), posing new questions and challenges in their effective implementation. The present paper firstly discusses the needs of low-distance-based sensors for indices calculation and then focuses on development of a new multispectral instrument, namely MAIA, specially developed for agricultural multispectral analysis. Such instrument features high frequency and high resolution imaging through nine different sensors (1 RGB and eight monochromes with relative band-pass filters, covering the range from 390 to 950 nm). The instrument allows synchronized multiband imaging owing to integrated global shutter technology, with a frame rate up to 5 Hz, and the exposure time can be as low as 1/5000 s. An applicative case study is eventually reported on an area featuring different materials (organic and non-organic), to show potential of the new instrument.

Keywords: wavelengths, vegetation indices, multiband imaging, synchronized, measurement

Citation: Dubbini, M., A. Pezzuolo, M. D. Giglio, M. Gattelli, L. Curzio, D. Covi, T. Yezekyan, and F. Marinello. 2017. Last generation instrument for agriculture multispectral data collection. *Agricultural Engineering International: CIGR Journal*, 19(1): 87–93.

1 Introduction

The effects of the interaction between the solar radiation and soil or vegetation are of great interest in agriculture, thanks to the possibility of collecting information with non-contact instrumentation. Specifically, remote or proximal sensors can collect

reflected electromagnetic radiation from a given surface, which typically depends on incident radiation and is inversely proportional to that absorbed by the same surface (e.g. plants or ground). Sensed data can be used to collect fast information at ground level (Sofia et al., 2016; Mavrakakis et al., 2014).

With specific reference to vegetation, two main wavelengths intervals can be identified (Mulla, 2013; Taghadomi-Saberi and Hemmat, 2015; Ghosh et al., 2015): in the visible spectrum (390-700 nm) plants typically exhibits high absorption characteristics, mainly ascribable to chlorophyll, anthocyanin's, carotenoids or

Received date: 2016-08-05 **Accepted date:** 2017-01-16

* **Corresponding author:** Francesco Marinello, Department of Land, Environment, Agriculture and Forestry, University of Padova, 35020 Legnaro, Padova, Italy. Email: francesco.marinello@unipd.it. Tel: 39 049 8272722. Fax: 39 049 8272750.

other pigments presence, and in the near infrared spectrum (700-2500 nm) reflectance is higher mainly due to multiscattering processes that occur within the structure of leaves.

The different behavior occurring in the visible and NIR regions intervals can be used in order to extract and collect information related to the photosynthetic pigments, whose activity is typically correlated to the physiological conditions of vegetation and thus provides indications on biomass, leaf area, health status, stresses, anomalies, etc., benefitting agricultural operations such as seeding or fertilization (Basso et al., 2016; Marinello et al., 2015). Indeed, a number of indices has been developed and proposed, based on calculations of reflectance values at wavelengths chosen in the two intervals (Bannari et al., 2007; Li et al., 2010; Miao et al., 2009; Mulla, 2013). Normalized Difference Vegetation Index (NDVI) is certainly the most common and well-known: according to Scopus database, it is cited in the title, abstract or as a keyword of over 12,000 scientific papers, but other indices are present in over 18,000 scientific papers.

As mentioned, contactless measurement has been one of the driving forces behind the studies on electromagnetic radiations on soil and plants (Karimi et al., 2015). Non-contact optical instruments can be therefore mounted at different distances from the surface of interest, varying from some hundreds of kilometers (as in the case of satellites) to some hundreds or tens of meters (as in the case of manned or unmanned aerial vehicles), down to less than one meter (proximal sensing with ground based platforms). Following the constant reduction in optical sensing (Marinello et al., 2008) particularly in the last few years, a great interest is raising around lightweight and small instruments, mainly due to the possibility to load onboard of drones or machinery (Candiago et al., 2015). Indeed, this can open up to the possibility of filling the gap and allowing high spatial resolution spectral imaging, with almost unconstrained return frequency.

Many instruments have been proposed in the last few years, allowing measurement at multiple wavelengths (from 4 to 25 bands) with high resolution (from 0.08 to 2 Mpixels) and featuring reduced weight (typically lower

than 500 g) with interesting performances also in terms of frame rate (Hill and Clemens, 2015). Some examples are those produced for instance by Tetracam, Sentek, Headwall, BaySpec, etc. (Berni, 2009).

2 Materials and methods

In the present paper the development of a new multispectral instrument is proposed. The new instrument, namely MAIA, features an array of nine sensors with 1.2 Mpixel resolution: specifically, 1 RGB color and eight monochrome sensor are available for analysis of the VIS-NIR spectrum from 390 to 950 nm, operating with a frame rate of 5 Hz per sensor. The dimensions of the sensors are 3.6×4.8 mm, with a 3.75 μm pixel size. Each of the eight sensors is provided with a band-pass filter (Table 1), but the specific configuration of the camera is designed for relatively fast exchange of filters for customized needs. Global shutter technology is implemented: thanks to this solution, all of the pixels in each sensor start to collect charge simultaneously allowing images to be scanned in “one shot” for synchronized multiband measurements. Exposure time can be as low as 1/5000 s.

Table 1 Instrument monochrome sensors with relative band-pass filters

| | Wavelength, nm | | | Full width at half maximum, nm |
|-----|----------------|---------|------|--------------------------------|
| | Start | Central | Stop | |
| 395 | 422.5 | 450 | 55 | |
| 455 | 487.5 | 520 | 65 | |
| 525 | 550 | 575 | 50 | |
| 580 | 602.5 | 625 | 45 | |
| 630 | 660 | 690 | 60 | |
| 705 | 725 | 745 | 40 | |
| 750 | 785 | 820 | 70 | |
| 825 | 887.5 | 950 | 125 | |

The horizontal and vertical angles of view for the system are respectively 33.4 and 25.5 degrees, with a nominal focal length of 7.5 mm (fixed lens). This corresponds to an imaged area of 45×35 m² with a ground sampling distance of 36 mm at 75 m height above ground and of 6×4 m² with a ground sampling distance of 5 mm at 10 m height.

Images are stored in an internal solid-state storage medium (120 Gb SSD) that provides high speed and the

possibility to save about 10,000 images in the maximum format allowed (12-bit raw). Considering an overlapping between images of 50% and a ground sampling distance of 3.5 cm, this corresponds to a potential maximum area of over 700 sampled hectares. The instrument is suited for unmanned aerial vehicles transportation, thanks to its reduced dimensions ($99 \times 128 \times 46 \text{ mm}^3$) and weight (400 g).

A schematic view of the instrument is proposed in Figure 1, where r.c.s. indicate the remote control signals coming from the operator and sent to the central processing unit (CPU). Data collected from the array of RGB and monochromatic sensors are processed by the CPU and sent to the operator monitor. RX and TX indicate respectively receiver and transmitter. The instrument can be interconnected with different global navigation satellite systems: GPS L1 or L1/L2, GLONASS, Galileo or Beidou, for an accurate log of synchronized shutter positions (available in PPP, PPK,

RTK). GNSS data are sent in a standard format (NMEA string) to the CPU; synchronization is ensured by a feedback loop (indicated by sync in and sync out). The user can interact with the camera to configure operating parameters and to manage the images both through the Giga Ethernet port and through integrated Wi-Fi. Instrument settings can be configured through the dedicated keypad using the On-Screen Display on the Video output port. The system can be stabilized by means of a gimbal that can get the positioning data directly from the on-board inertial measurement unit (IMU) for maximum precision. Co-registration process is based on specific alignment parameters computed in a laboratory calibration process which considers each of the nine optical elements and sensors of the camera. The instrument is completed by an included pre-processing software tool, which permits merging the images of each single band on one multispectral image with the pixel-convergence.

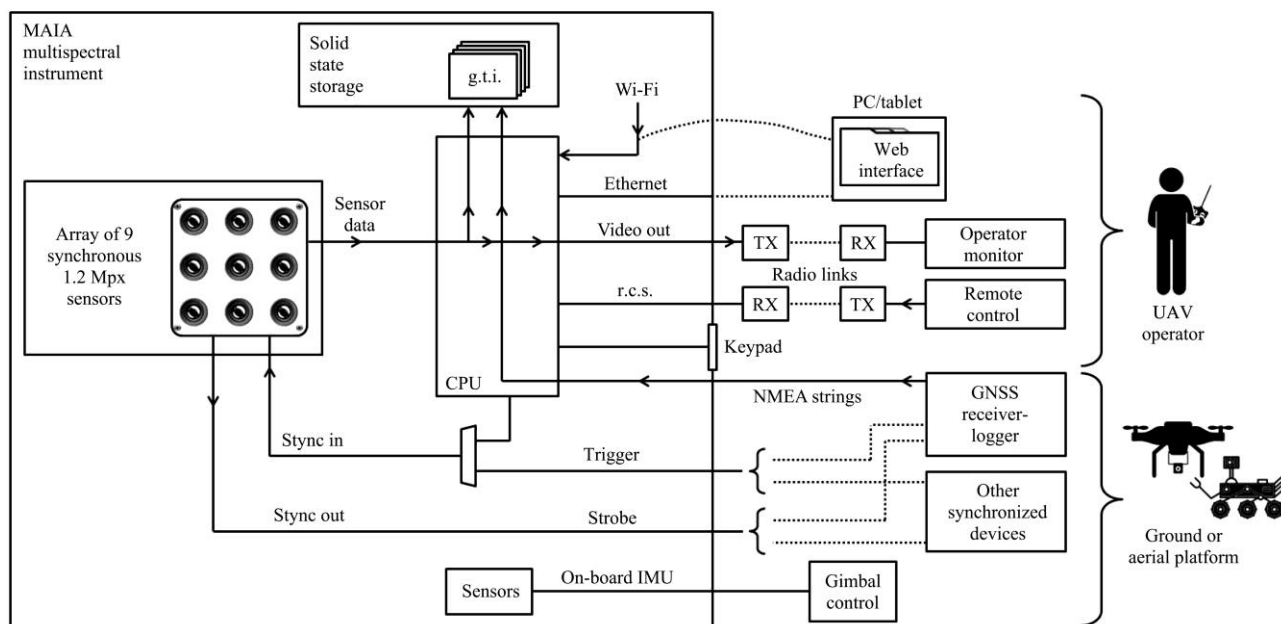


Figure 1 Schematic representation of the proposed MAIA instrument

2.1 Indices coverage

As discussed in the previous paragraph, the new multispectral instrument has been designed in order to allow the maximum flexibility in terms of characterization capability in the agricultural field, opening to the possibility of quantifying a large number of vegetation indices. In Figure 2 the eight bands of the monochrome sensors are represented (namely BP1 -BP8), together with

the wavelengths occurrences in 81 different vegetation indices, as reported in literature (Bannari et al., 2007; Li et al., 2010; Miao et al., 2009; Mulla, 2013). From the histogram it appears how the eight bands cover the most important wavelengths, particularly 550 nm (occurring in 20 indices), 670 nm (in 19 indices) and 800 nm (in 22 indices).

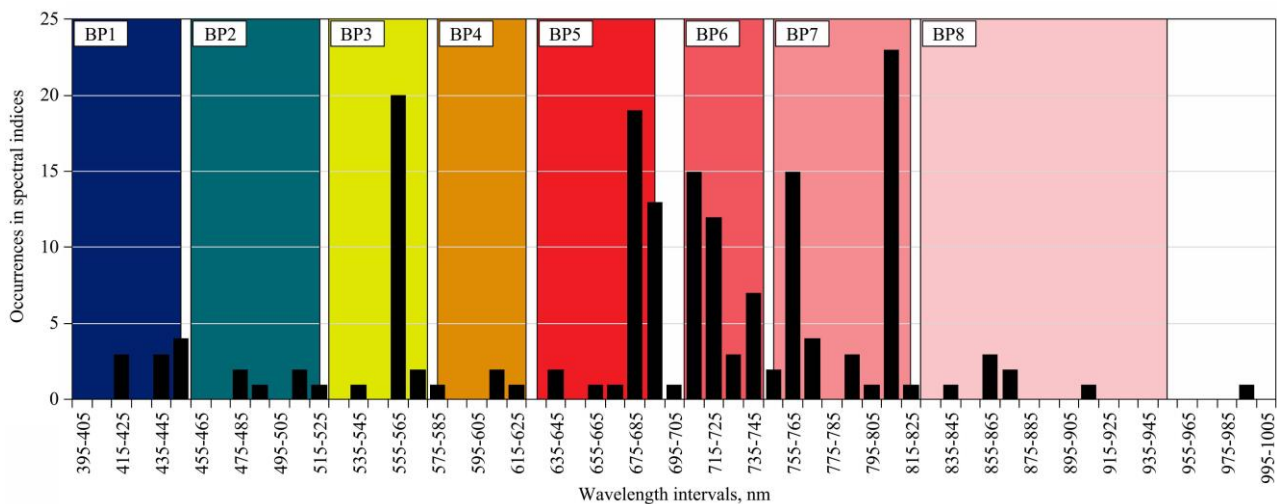


Figure 2 Wavelengths occurrences in spectral indices and band coverage by the proposed instrument

Considering the central wavelength of the eight bands, with a tolerance of ± 5 nm, 16% of the indices can be properly computed; increasing the tolerance at ± 15 nm or ± 20 nm, the percentage raises respectively at 31% and 52% of the indices; considering the full width at half maximum, 72% of the indices can be computed (Table 2).

Table 2 Indices coverage considering different band widths on the central wavelengths of the proposed instrument

| Band width on the central wavelength | Indices coverage |
|--------------------------------------|---|
| ± 5 nm | NDVI3, NG, NR, NNIR, RVI, GRVI, DVI, GDVI, SAVI, GSAVI, GOSAVI, MSAVI2, GMSAVI2 |
| ± 15 nm | SR2, DI1, OSAVI, RDVI, MSR, MSAVI, MTVI, MCARI2, CAI, NPQI, SR15, NDVI4 |
| Full width at half maximum | Greenness index (G), SR1, SR4, SR6, NDVI, GNDVI, PSSRa, ND11, PRI, SRPI, NPCI, PSNDa, PSNDc, PSSRc, SR11, SR18, NDVI8 |
| ± 20 nm | SR7, PSSRb, NDI2, SIPI, HNDVI, MTCI, PSNDb, Viopt2, SR8, SR12, SR13, SR17, Viopt1, RGR, NDVI6, NDVI7 |
| Out of full width half band | SR3, SR5, NDI3, MCARI, TCARI, TVI, CARI, ZTM, mND705, mSR705, SR9, SR10, SR14, SR16, DD, R-M, G-M, ND705, PSRI, NDIV1, NDVI2, NDVI5, REIP |

3 Results and discussion

3.1 Sensors performance

In the present paragraph some aspects of the new instrument performance are discussed. Figure 3 shows the Quantum Efficiency curve $QE(\lambda)$ of the imaging sensor weighted by the Transmittance curve $T(\lambda)$ of the bandpass filters. The product between these two quantities is the key figure related to the light detection efficiency of the camera. The QE data are provided by the

sensor manufacturer, while the transmittance has been measured by means of a spectrophotometer on the filters actually used.

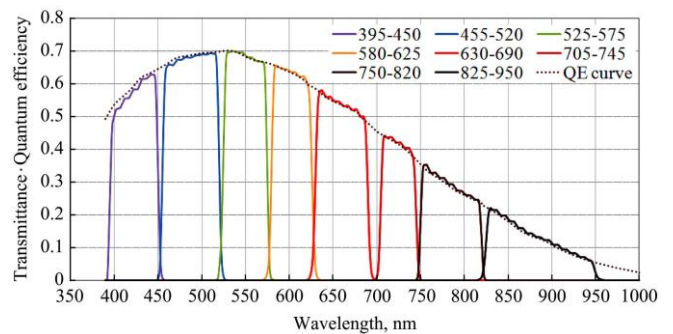


Figure 3 Wavelengths occurrences in spectral indices and band coverage by the proposed instrument

Other elements in the optical path are the protective glass window and the lens. They feature a flat transmittance across the wavelength range of interest and have therefore been neglected in the calculations. The bandpass filters have been custom designed in order to optimize their performance and achieve high transmittance within the band, steep transition from the pass-to blocking-region and no overlap between adjacent bands. The in-band transmittance of the filters is in average higher than 90%. This feature allows to fully exploit the excellent quantum efficiency of the sensors, which is one of the highest currently available efficiencies on the market. The transition between $T=10\%$ and $T=90\%$ is approximately 5 nm and therefore the gap between the band is so small that the full VIS-NIR spectrum can be effectively explored.

One important aspect with regards to the practical use

of the camera is the area underneath the curve $QE \cdot T$ (Figure 4). The area is the integral of all photons that hits the sensor and that can be converted into an electric signal. The larger the area, the higher the signal and brighter the image.

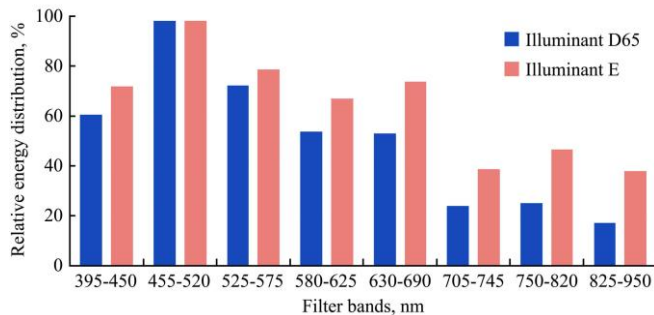


Figure 4 Relative energy distribution for different wavelength bands

The number of photons reaching the sensor in each band also depends on the spectrum of the light source that illuminates the observed target and the reflectance of the target itself. By choosing a certain illuminant and reflectance spectrum, it is possible to estimate what is the expected energy distribution of the photons among the bands and, by integration over wavelengths, calculate the expected signal that the camera will detect.

It is important that the difference between the highest and the lowest signal is as low as possible. A difference between these values turns into a difference in the integration times that has to be used by the sensor in order to obtain the same digital number while detecting them. Having images with the same average digital number is not mandatory for the proper calculation of a certain index.

However, it is a constraint that is often implicit in real-life operations, when a camera shot in auto-exposure mode. In this case, the sensor that receives the lowest amount of light needs the longest integration time and becomes the bottleneck of the system because it sets the limit for the maximum speed that the UAV can travel without having motion blur in the images. An estimation of the ratio between the signals in the various bands (keeping the highest as divider) has been calculated under the following assumptions:

- The illuminant is the average midday light of the sun at European latitude (D65, according to ISO 10526:1999/CIE S005/E-1998 standard); this is not

only a well-known illuminant but also in agreement with the very likely operating scenario of the system. Also the equal-energy illuminant E has been considered for reference.

- The reflectance of the target is 100% across the wavelength range, which is equivalent of having a perfectly white target; such reflectance curve (differently from others like those of vegetation, soil or water) is interesting due to its independency from the specific application.

Results are depicted in Figure 4, and show how the bands in the visible range are expected to gather a similar signal. Specifically, in the visible region a factor lower than two is detected between the highest and lowest bands, while in the near infrared region, the rate increases up to a factor of five (Figure 5). This is due to the combination of two elements:

- The decrease of QE in the NIR region, typical of a silicon-based detector
- The fact that the NIR region is split in three bands and therefore the available energy is shared on three sensors.

The latter has been a design choice that is needed in order to maximize the above mentioned instrument flexibility in indices calculation.

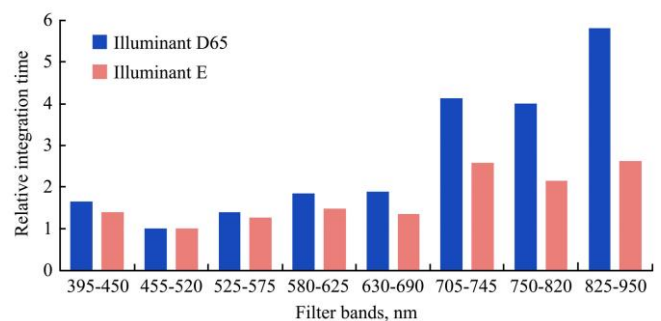


Figure 5 Relative integration times for different wavelength bands

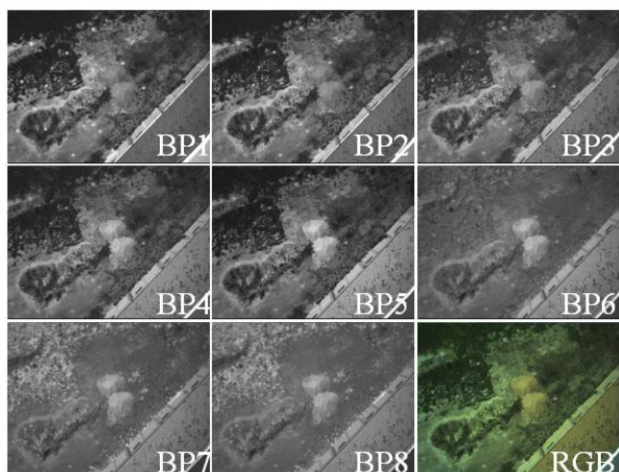
3.2 Field application

The first field test analysis for the evaluation of the instrument performance was carried out. Tests were performed considering the acquisition of the pseudo-nadir images with the sensor installed on board a four-rotor unmanned aerial vehicle (Figure 6a). The radio-controlled quadcopter was operated in an area featuring different physical conditions on the ground (Figure 6b). The chosen site was heterogeneous both in

terms of materials (grass, bare soil, asphalt, brick, etc.) and ground conformation (different relative heights and different dimension). Reference spots (fiducial marks) were positioned on the ground in order to test the ability of the instrument to align the nine images.



a. MAIA sensor installed on board a drone



b. Signal collected by the nine sensors

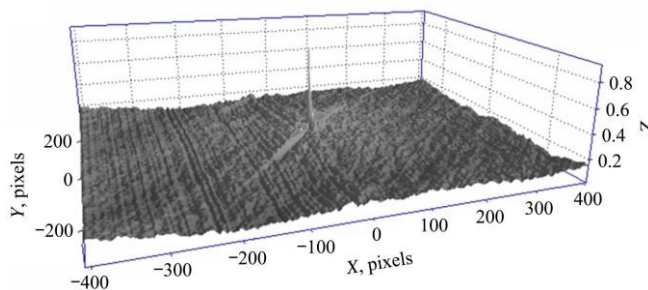
Figure 6 New instrument during field measurements

In order to assess the quality of the co-registration process, the images from the nine sensors (Figure 6b) were post-processed in order to calculate the average normalized cross-correlation, as reported in Figure 7a. Cross-correlation function describes the statistical similarity between two images, and values close to one are indicative of an ideal degree of correspondence (Van der Meer, 2006).

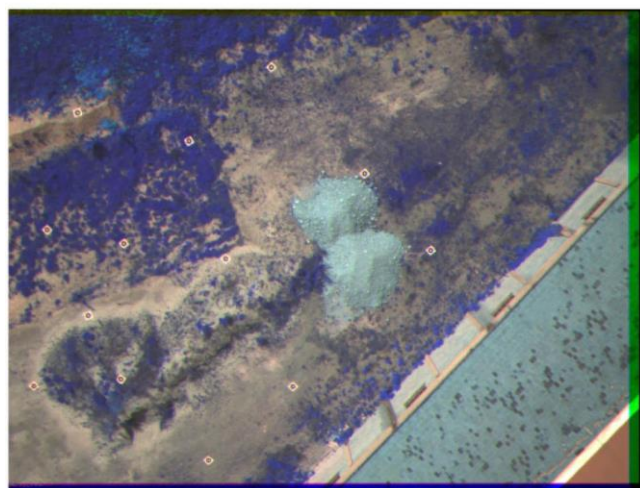
For the scope, images underwent normal gradient calculation and subsequent binarization, in order to highlight borders and fiducial marks, and eliminate differences intrinsically present due to the different signal collected at different wavelength. Cross-correlation was then computed for any given couple of scans picked

between the nine collected for a total of 36 controls per measurement. An average value higher than 0.99 was detected and values higher than 0.97 were in general detected for any given couple of scans. This correspond to an average shift between different scans which is in general comprised between 0.1 and 0.4 pixels, with an average misalignment as low as 0.14 pixels.

Such good correlation is at a basis of the possibility to generate a multi-layer product as a result of aligned scans taken at different wavelengths (Figure 7). This is a primary condition when vegetation indices have to be computed from multispectral measurements and pixel or even sub-pixel accuracy is needed to allow specific localization of extracted indices.



a. Average cross-correlation function



b. Multilayer result

Figure 7 Result of the co-registration process

4 Conclusions

The present paper focuses on the development of a new instrument allowing exploitation of multispectral measurements, covering the visible and near-infrared range (from 390 to 950 nm). The main features of the proposed instrument include:

- a relatively high and well distributed number of wavelength bands (eight monochromatic and 1 RGB),

useful for determination of a large number of spectral indices;

- implementation of a global shutter technology which allows collection of images with a high level of accuracy with respect to alignment (average cross-correlation higher than 0.995);
- custom designed filters characterized by high transmittance within the band, steep transition from the pass- to blocking-region and no overlap between adjacent bands;
- homogeneous relative energy distribution and low integration time disparity between different detected bands, especially in the visible field;

High resolution imaging, high frequency frame rate and relatively low dimensions and weight give the new instrument ideal characteristics for ground or aerial sensing to exploit vegetation indices extrapolation in agricultural applications.

Acknowledgements

The activity of Francesco Marinello and Andrea Pezzuolo is supported by a grant from the University of Padova (code CPDA143174), Italy.

References

- Bannari, A., K. S. Khurshid, K. Staenz, and J. W. Schwarz. 2007. A Comparison of hyperspectral chlorophyll indices for wheat crop chlorophyll content estimation using laboratory reflectance measurements. *IEEE Transactions on Geoscience and Remote Sensing*, 45(10): 3063–3074.
- Basso, B., B. Dumont, D. Cammarano, A. Pezzuolo, F. Marinello, L. Sartori. 2016. Environmental and economic benefits of variable rate nitrogen fertilization in a nitrate vulnerable zone. *Science of the Total Environment*, 545-546: 227–235.
- Berni, J. A. J., P. J. Zarco-Tejada, L. Suarez, and E. Fereres. 2009. Thermal and narrowband multispectral remote sensing for vegetation monitoring from an Unmanned Aerial Vehicle. *IEEE Transactions on Geoscience and Remote Sensing*, 47(3): 722–738.
- Candiago, S., F. Remondino, M. De Giglio, M. Dubbini, and M. Gattelli, 2015. Evaluating multispectral images and vegetation indices for precision farming applications from UAV images. *Remote Sensing*, 7(4): 4026–4047.
- Ghosh, S., T. R. C. Domínguez, B. Diezma, L. Lleó P. Barreiro, T.G. Lacarra, and J.M. Roger. 2015. VIS/NIR spectral signature for the identification of peanut contamination of powder foods. *CIGR Journal*, 17(2): 310–329.
- Hill, S. L., and P. Clemens. 2015. Miniaturization of high spectral spatial resolution hyperspectral imagers on unmanned aerial systems. In *Proceedings of the SPIE 9482, Next-Generation Spectroscopic Technologies VIII. 94821E*.
- Karimi, H., H. R. Ghassemzadeh, P. Pashae, and E. Z. Shahamat. 2015. Proposing an appropriate soil water content estimation technique for Iran. *CIGR Journal*, 17(2): 1–10.
- Li, F., Y. Miao, S. D. Hennig, M.L. Gnyp, X. Chen, L. Jia, and G. Bareth. 2010. Evaluating hyperspectral vegetation indices for estimating nitrogen concentration of winter wheat at different growth stages. *Precision Agriculture*, 11(4): 335–357.
- Marinello, F., E. Savio, S. Carmignato, and L. De Chiffre, 2008. Calibration artefact for the microscale with high aspect ratio: The fiber gauge. *CIRP Annals - Manufacturing Technology*, 57(1): 497–500.
- Marinello, F., A. Pezzuolo, F. Gasparini, J. Arvidsson, and L. Sartori. 2015. Application of the Kinect sensor for dynamic soil surface characterization. *Precision Agriculture*, 16(6): 601–612.
- Mavrakis, A., A. Colantoni, and L. Salvati. 2014. Soil degradation, landscape and climate variations in a Mediterranean agro-forest system (Thriasio, Greece): proposal for a desertification indicator using time series analysis. *International Journal of Agricultural Resources Governance and Ecology*, 10(4): 335–343.
- Miao, Y., D. J. Mulla, G. W. Randall, J. A. Vetsch, and R. Vintila. 2009. Combining chlorophyll meter readings and high spatial resolution remote sensing images for in-season site-specific nitrogen management of corn. *Precision Agriculture*, 10(1): 45–62.
- Mulla, D. J. 2013. Twenty-five years of remote sensing in precision agriculture: Key advances and remaining knowledge gaps. *Biosystems Engineering*, 114(4): 358–371.
- Sofia, G., F. Marinello, and P. Tarolli. 2015. Metrics for quantifying anthropogenic impacts on geomorphology: Road networks. *Earth Surface Processes and Landforms*, 41(2): 240–255.
- Taghadomi-Saberi, S., and A. Hemmat. 2015. Improving field management by machine vision - A review. *CIGR Journal*, 17(3): 92–111.
- Van der Meer, F. 2006. The effectiveness of spectral similarity measures for the analysis of hyperspectral imagery. *International Journal of Applied Earth Observation and Geoinformation*, 8(1): 3–17.